# Modulation Schemes for Single-Laser 100 Gb/s Links: Single-Carrier

Milad Sharif, Jose K. Perin, and Joseph M. Kahn, *Fellow, IEEE*

*Abstract*—We evaluate single-carrier modulation techniques for 100 Gb/s single-laser data center interconnects. We present numerical performance analysis for various single-carrier schemes including pulse amplitude modulation (PAM), carrierless amplitude phase modulation, and orthogonal multipulse modulation in the presence of optical modulator bandwidth limitations and nonlinearity, clipping, quantization noise, and fiber chromatic dispersion. The performance is evaluated in terms of the required average optical power to achieve a target bit-error ratio for a given modulator bandwidth. We compare the complexity of different designs in terms of the required resolution and sampling rate of digital-to-analog (DAC) and analog-to-digital (ADC) converters, as well as the number of complex operations required for digital signal processing. We find that 4-PAM is the most power efficient scheme among those considered, and that it can be implemented with DAC/ADC resolution as low as 5 bits.

*Index Terms*—Carrier-less amplitude phase modulation, communications system performance, data center interconnects, direct detection, intensity modulation, pulse amplitude modulation.

## I. INTRODUCTION

CURRENT standards for 100G links are based on modulating ten parallel optical lanes of 10 Gb/s or four lanes of 25 Gb/s using conventional non-return to zero modulation [1]. This approach, however, does not scale well to higher bit rates, as 400 Gb/s links would require 16 lanes of 25 Gbs/s [2], imposing severe drawbacks in terms of system cost, complexity and power consumption [1]. Power efficiency and optical component costs are the two most important design parameters for data center links.

Higher-order modulations have recently proposed [3], [4] to increase spectral efficiency and thus reduce the number of optical lanes. The general idea is to transmit 100 Gb/s per wavelength and use parallel optics to enable 400 Gb/s and possibly 1.6 Tb/s links. Several modulation schemes have been studied for 100 Gb/s, including pulse-amplitude modulation (PAM) [5], [6], carrierless amplitude and phase modulation (CAP) [7], [8], digital quadrature amplitude modulation (QAM) with an

optimized constellation [9], orthogonal multi-pulse modulation (OMM) or orthogonal PAM [10], and discrete multi-tone [4]. Previous works have compared some of these modulation methods through extensive simulations [7], [11], [12] or experimentally [13], but no study to date has provided a detailed analysis of these modulation techniques.

In this paper and a companion paper [14], we study various modulation formats for single-laser 100G links using analytical models. Here, we present a general system model for single-laser 100 Gb/s links based on single-carrier modulation. The model is formulated for short-reach interconnects in short lengths (typically up to 2 km) of standard single mode fiber (SMF). The model assumes intensity modulation with direct detection, in light of the cost and power consumption limitations in data center links.

We present numerical analysis for the performance and complexity of various single-carrier modulations and equalization schemes proposed for single-laser 100G links. Specifically, we study the effects of modulator bandwidth limitations and nonlinearity and clipping and quantization noises introduced by digital-to-analog and analog-to-digital converters (ADC and DAC) on system performance. We evaluate the performance based on required optical power for achieving a target bit-error ratio (BER) as a function of the modulator bandwidth. For optical powers near the ideal receiver sensitivity, the dominant noise source is thermal noise [14], [15].

In order to accommodate power penalties from impairments and receiver non-idealities and to provide margin for losses from connectors and patch panels, the launched power can significantly exceed the ideal receiver sensitivity, and other noise sources, such as clipping, quantization, shot noise and intensity noise, become important. Hence, we initially consider a thermal-noise-limited receiver with infinite DAC/ADC resolution in our analysis. Then, for the best modulation scheme, we present simulation results including other effects such as shot noise, intensity noise, chromatic dispersion (CD), and modulator chirp and nonlinearity. Finally, we establish design requirements for sampling rate and resolution of DAC and ADC. The resolution and sampling rate of DAC/ADC are of particular interest, since these components are the dominant source of power dissipation in data center interconnects [6].

The remainder of this paper is organized as follows. In Section II, we present the system model used in our analysis.

In Section III, we highlight key trade-offs in the design of a 100G link. We compare the requirements and complexity of various system components in Section IV. In Section V, we present simulations that confirm key assumptions made in the analysis. We present conclusions in Section VI.
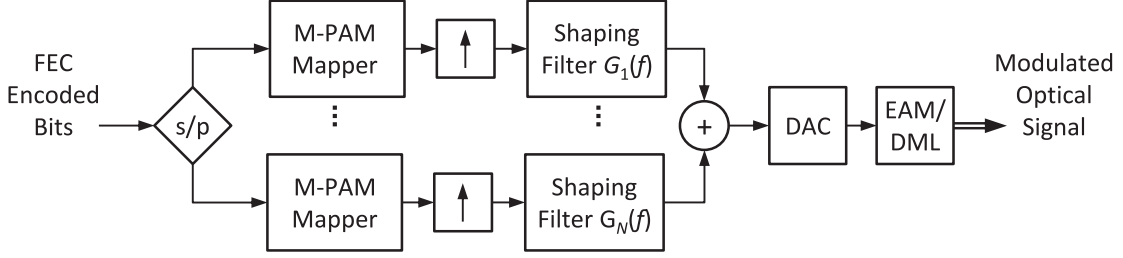
Fig. 1.  OPAM transmitter with $N$ parallel $M$-PAM mappers. The upsampling and digital pulse shaping blocks are not necessary for OPAM systems with $N = 1$.

## II. SYSTEM MODEL

### A. Orthogonal PAM Architecture

A general block diagram for an orthogonal PAM transmitter is shown in Fig. 1. PAM, CAP, and OMM all can be implemented using this architecture. At the receiver, multiple independent streams of input bits are mapped into $M$-level PAM symbols by $N$ parallel modulators. Symbols might then be up-sampled and passed through the digital pulse shaper. Non-rectangular pulse shaping is only necessary if the system has more than one subchannel, and can be avoided in PAM. Note that while Fig. 1 shows a digital implementation, orthogonal PAM can be implemented using either analog [10], [16] or digital filters [7], [9].

After filtering, shaped signals are combined and converted into analog signals. A dc bias is required to make the signal nonnegative to drive the optical modulator. We consider both directly modulated lasers (DMLs) and electro-absorption modulators (EAMs). DMLs offer lower cost and power consumption. DMLs are commercially available only with bandwidths up to about 25 GHz, although devices with bandwidths up to about 35 GHz have been demonstrated experimentally [17]. EAMs generally have higher bandwidth, but known to be sensitive to temperature variation [18].

DMLs can be modeled by a second-order linear system, which follows directly from solving the laser rate equations. For EAMs, the bandwidth-limiting factor is parasitic capacitance and inductance. EAMs are typically modeled as lumped-element circuits with two dominant poles [19]. Hence, both DMLs and EAMs are modeled here by a two-pole linear system $H_{\mathrm{mod}}(f)$, with cutoff frequency $f_{\mathrm{3dB}}$ and damping constant of unity. Since the cutoff frequency $f_{\mathrm{3dB}}$ is significantly less than the bit rate, the modulator poses a significant bandwidth limitation, which is the major impairment of 100G links. Modulator nonlinearity is not included in our analytical model, but is included in the system simulations presented in Section V.

After propagating through the fiber, the received signal is direct detected, and amplified by the transimpedance amplifier (TIA). Typical TIAs have 3-dB cutoff frequencies of 20–70 GHz and input-referred noises $I_{n,in}$ of 20–50 pA/$\sqrt{\mathrm{Hz}}$, where the input-referred noise is related to the power spectral density of the thermal noise by $N_0 = I_{n,in}^2$ [38].

The CD of fiber is expected to be negligible, as 100G interconnects operates near the zero-dispersion wavelength in short lengths of fiber. The simulations in Section V confirm that CD has negligible impact even in 400G links using four wavelengths over a transmission distance of 2 km.

The received signal is then sampled and quantized by an ADC. The signal might be clipped to reduce the dynamic range required of the ADC. Since the transmitted pulse shapes in different subchannels are orthogonal, a bank of matched filters is used in an effort to separate the subchannels. Digital signal processing (DSP) is further required to compensate for the interference introduced by modulator bandwidth limitations.

As in the transmitter, the receiver matched filters can be implemented in the digital or analog domain. A digital implementation can exploit fractionally spaced equalization, at the cost of higher sampling rate and higher power consumption. Although digital and analog implementations of the receiver differ significantly in complexity and component requirements, they have similar performance on bandwidth-limited AWGN channels.

### B. Discrete-Time Model

As mentioned before, for optical powers near the receiver sensitivity, thermal noise is dominant. Therefore, we consider a thermal noise limited receiver with infinite DAC/ADC resolution for calculation of receiver sensitivity, and include quantization noise subsequently. Neglecting fiber and modulator nonlinearity, the system can be modeled as a linear system. As we show in Section V, including other effects such as intensity noise, shot noise, chirp, and CD has a little impact on system performance.

Ignoring distortion caused by anti-aliasing filter and finite DAC resolution, the transmitted signal can be written as

$$s(t) = \sum_{n} \sum_{i=1}^{N} a_n^i h_i(t - nT_s), \tag{1}$$

where $\{a^i\}$ is the sequence of transmitted symbols in the $i$th orthogonal subchannel, $1/T_s$ is the symbol rate, and $h_i(t) = g_i(t) * h_{\mathrm{mod}}(t)$. Assuming an ADC with Nyquit-rate sampling, we can interchange the order of sampling and the matched filter. Hence, the sampled output of the $i$th orthogonal subchannel is given by

$$r_k^i = a_k^i + \sum_{n \neq k} a_n^i x_{k-n}^{(ii)} + \sum_{\substack{j=1 \\ i \neq j}}^{N} \sum_{n} a_n^j x_{k-n}^{(ij)} + \eta_k^i, \tag{2}$$

where $x^{ij}$ is the sampled cross-correlation of $h_i(t)$ and $h_j(t)$ and $\eta^i$ is the colored Gaussian noise sequence at the matched
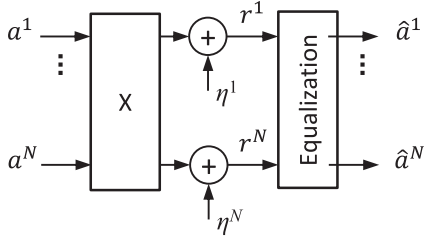
Fig. 2.　Equivalent discrete-time block diagram of OPAM sampled at the symbol rate.

filter output. Fig. 2 shows the discrete-time model of an orthogonal PAM system. As indicated by (2), received samples are corrupted by inter-symbol and inter-channel interference in addition to the Gaussian noise. As in any practical system, we assume that the interference affects a finite number of symbols. Hence, we assume that $x_n = 0$ for $|n| > L$, where $L$ is the memory length of the channel.

In the absence of the interference, the symbol error rate of orthogonal PAM, can be derived analytically as a function of the average optical power [20]:

$$\text{SER} = \frac{2(M-1)}{M} Q \left( \sqrt{\frac{\log_2 M}{N(M-1)^2} \frac{R^2 P^2}{R_b N_0}} \right), \quad (3)$$

where $R_b$ is the bit rate and $R$ is the photodiode responsivity. For comparison of various schemes, we consider the required average optical power of the system with $R_b = 100$ Gb/s (excluding coding overhead) to achieve a target BER of $10^{-12}$. The system is assumed to use a Reed-Solomon code with a coding gain of 5.6 dB and requiring an input BER of $1.8 \times 10^{-4}$ to achieve an output BER of $10^{-12}$ [21].

In order to eliminate the dependency of the results on the thermal noise characteristics of the receiver, we normalize the average optical power by the optical power required for a coded OOK system. The normalized required optical power, assuming an optical modulator with ideal extinction ratio, can be approximated by

$$\frac{\overline{P}_{req}}{\overline{P}_{OOK,req}} = (M-1)\sqrt{\frac{N}{\log_2 M}}. \quad (4)$$

The extinction ratio $r_{ex}$ is defined as the ratio between the minimum and maximum modulator output powers. A non-ideal extinction ratio causes an additional penalty of approximately

$$\Delta \overline{P}_{ex} = \frac{1 + r_{ex}}{1 - r_{ex}}. \quad (5)$$

in the thermal-noise-dominated regime. The penalty due to a finite $r_{ex}$ is independent of PAM order, and is negligible for modulators with $r_{ex}$ of $-12$ to $-15$ dB [6].

The average optical power is limited to 9.4 dBm due to the eye-safety restrictions [22]. Therefore, for 400G links with four WDM channels the maximum average optical power per channel is limited to 3.4 dBm. Assuming an input-referred noise of 30 pA/$\sqrt{\text{Hz}}$, and a target BER of $1.8 \times 10^{-4}$, we have

$P_{OOK,req} = -16.1$ dBm. Hence, assuming link attenuation up to 5 dB, penalties up to 14 dB are tolerable.

## III. System Design Trade-offs

In order to increase the bit rate per wavelength and therefore reduce the number of optical lanes, one can increase the constellation size, or the multiplexing factor of an orthogonal PAM system. In this section we highlight the key trade-offs in the design of 100G links.

### A. Equalization

Digital equalization is necessary to eliminate the interference introduced by optical modulator bandwidth limitations. Bandwidth limitations can be compensated either by transmitter-side pre-emphasis filtering or receiver-side digital equalization. In numerical analysis, we assume a symbol-rate equalizer, which is optimum if the matched filter is matched to the received pulse shape, i.e., the overall response of the pulse shaper and optical modulator. However, a symbol-rate receiver is sensitive to sampling time error. Moreover, the exact response of the modulator might be unknown. Hence, in practice, the receiver filter is often matched to the transmitted pulse shape and the sampling rate is adjusted for this suboptimum filter. With high enough oversampling rate, a fractionally spaced equalizer (FSE) has performance similar to the optimum receiver [23]. In the case of FSE, the discrete-time matched filter and equalizer are generally combined into a single filter. In our analysis, we assume symbol-rate equalization with perfect knowledge of the channel. We consider both maximum likelihood sequence detection (MLSD) and much simpler linear equalization (LE) or decision-feedback equalization (DFE) with symbol-by-symbol detection.

It is well known that the optimum detector for PAM in additive Gaussian channels with bandwidth limitation is MLSD, which can be implemented using the Viterbi algorithm preceded by a noise whitening filter [24]. At high SNR, the probability of symbol error for PAM can be well approximated by

$$\text{SER} \approx k_\delta Q \left( \sqrt{\frac{\log_2 M}{(M-1)^2} \frac{R^2 P^2}{R_b N_0} \delta_{\min}^2} \right), \quad (6)$$

$$\delta_{\min} = \min_{\{\varepsilon_k\}} \sum_{i=0}^{\infty} \left( \sum_{j=0}^{\infty} f_j \varepsilon_{i-j} \right)^2, \quad (7)$$

where $k_\delta$ is a weighting factor describing the average number of symbol errors per sequence, $f_n$ is the response of the noise whitening filter to $x_n$ and minimization is performed over all possible error sequences $\{\varepsilon_k\}$ starting at time zero. For low SNR we rely on simulation to estimate the optical penalty.

MLSD for systems with more than one channel has been studied in the context of multiuser interference cancellation [25], [26]. Although MLSD can optimally decode multiple subchannels in parallel, its computational complexity grows exponentially with the channel memory length $L$ and the number of channels $N$. Such large computational complexity is not practical in data center interconnects having tight power consumption budgets. Suboptimal equalization techniques, such as LEs and

DFEs are significantly less complex and consequently, more desirable for interconnects applications. Detailed analysis of performance of different equalization techniques for PAM is given in [23]. Here we generalize the analysis in [23] for orthogonal PAM systems. Assuming a minimum mean-square error LE with coefficients $c_n^{(ij)}$ for $i, j = \{1, \ldots, N\}$, the output of the equalizer can be written as

$$\hat{a}_k^i = q_0^{(ii)} a_k^i + \sum_{n \neq k} a_n^i q_{k-n}^{(ii)} + \sum_{\substack{i,j=1 \\ i \neq j}}^{N} a_n^j q_{k-n}^{(ij)} + v_k^i, \quad (8)$$

where

$$q^{(ij)} = \sum_k x^{(kj)} * c^{(ik)} \quad (9)$$

and $\nu^i$ is a white Gaussian noise with the variance of

$$\sigma_i^2 = N_0 \sum_{j=1}^{N} \sum_n \left( c_n^{(ij)} \right)^2. \quad (10)$$

For a particular symbol sequence of length $l$, the conditional probability of error for the $i$th subchannel is given by

$$P_e^{(i)}(D) = 2 \frac{M-1}{M} Q \left( \sqrt{\frac{(q_0 - D)^2}{\sigma_i^2}} \right), \quad (11)$$

where

$$D = \sum_{n \neq k} a_n^i q_{k-n}^{(ii)} + \sum_{\substack{i,j=1 \\ i \neq j}}^{N} a_n^j q_{k-n}^{(ij)}. \quad (12)$$

By averaging over all possible sequence and subchannels, assuming sequences of equiprobable symbols, we have

$$\text{SER} = 2 \frac{M-1}{M} \frac{1}{N \cdot M^l} \sum_{i=1}^{N} \sum_{\substack{\text{all possible} \\ \text{sequence}}} Q \left( \sqrt{\frac{(q_0 - D)^2}{\sigma_i^2}} \right). \quad (13)$$

Fig. 3 shows the optical power penalty for 4-PAM with different equalization techniques. We can observe that the penalty of using suboptimal equalizers is not significant and the complexity of MLSD can be avoided at a small cost. While the performance of DFE is better than LE, it is subject to error propagation. Error bursts can reduce the coding gain provided by FEC. Precoding at the receiver or block interleaving can break up the error bursts, but the additional latency might not be acceptable. Also, implementing a feedback filter with multiple taps at such a high rate might not be practical [9]. Hence for the rest of the paper we assume LE at the receiver.

### B. Symbol Rate

One of the main challenges of 100G links is performing DSP at very high sampling rates. Hence, systems with lower symbol rate are generally more desirable. One can reduce the symbol rate by increasing the constellation size. Systems with higher constellation size require less bandwidth and thus, are more tolerant of modulator linear distortion. Fig 4 shows the optical
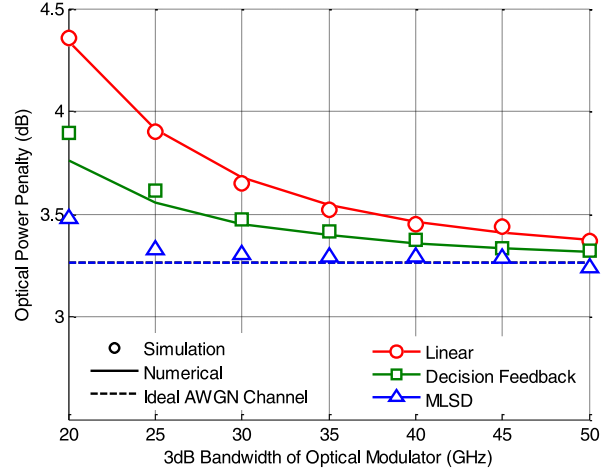


Fig. 3. Normalized optical power penalty for 4-PAM systems with different equalization techniques. The dashed line corresponds to the optical power penalty on an ideal AWGN optical channel given by (4).
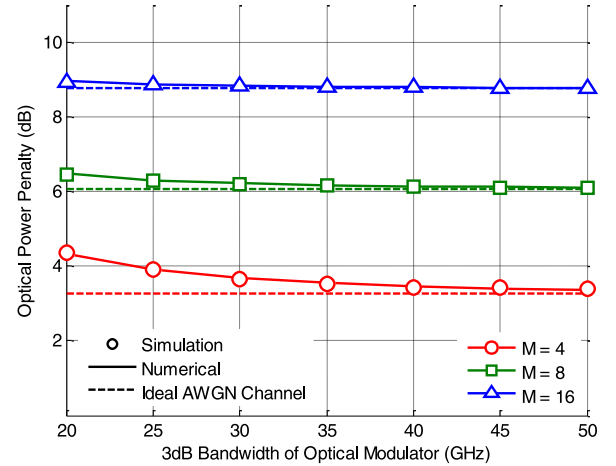


Fig. 4. Normalized optical power penalties for different PAM orders using LE. Dashed lines correspond to the optical power penalty on an ideal AWGN optical channel given by (4).

power penalty for 100G $M$-PAM systems with different constellation sizes. It can be seen that as we increase $M$, the interference penalty becomes negligible to the point that we might be able to avoid equalization. However, high-order PAM systems have a high optical power penalty and, as we show in Section IV, have more stringent ADC/DAC resolution requirements.

One can also reduce the symbol rate by increasing the number of orthogonal subchannels $N$. The optical power penalty is proportional to the square root of $N$, while it is almost linear in $M$. In fact, a system with the highest number subchannels has the lowest power penalty among OPAM systems with the same symbol rate. However, systems with more subchannels require significantly more bandwidth, and are more prone to modulator bandwidth limitations. For example, as shown in the Appendix, OMM requires a bandwidth exceeding 100 GHz. Throughout the paper, we assume an OMM system with four 2-PAM modulators, and rectangular waveforms based on Hadamard codes.
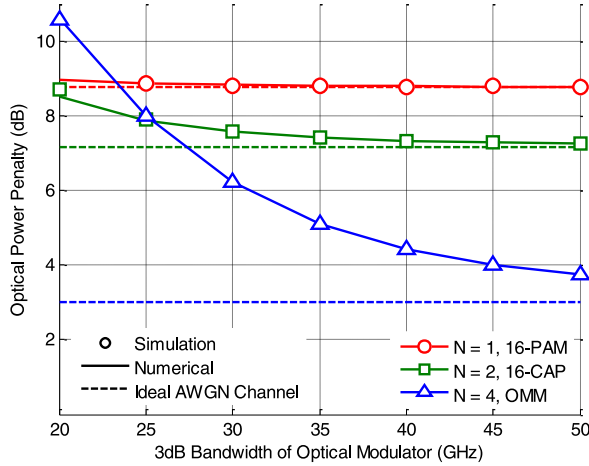
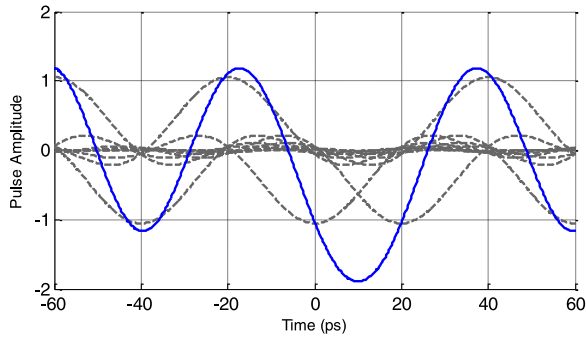Fig. 5. Normalized optical power penalty for OPAM systems with different number of subchannels using LE.



Fig. 6. Overlapping root-raised-cosine pulses with roll-off factor $\beta = 0.2$ over several symbol intervals. Individual pulses are shown by dashed lines. The solid line corresponds to a superposition of the individual pulses.

Fig. 5 shows the performance of three systems with symbol rate of 25 GBd and different numbers of subchannels. As we can see, for high modulator bandwidths, OMM has the best performance. However, as we decrease the modulator bandwidth, systems with fewer subchannels become more power efficient.

### C. Pulse Shaping

For systems with multiple subchannels, pulse shaping is necessary to make the subchannels separable at the receiver. Pulse shapes are constructed based on an orthogonal basis functions so that subchannels can be decoupled using a filter bank. In standard implementation of CAP, pulse shapes are based on root-raised-cosines multiplied by sinusoids. In PAM systems, pulse shaping is not required, but can be used to reduce the interference either by reducing the signal bandwidth or by pre-compensating for the modulator frequency response. However, shaped pulses can overlap in time and increase the peak value of the signal. Therefore, the required DC bias for the driver signal can increase. Fig. 6 shows overlapping root-raised cosine pulses over a period of several symbols. As can be seen, the minimum required dc bias is almost twice the peak value of individual pulses.

### TABLE I
PULSE SHAPING PENALTY FOR VARIOUS PULSE SHAPES

| Modulation | Pulse shapes | Shaping penalty (dB) |
|---|---|---|
| PAM | Root-raised-cosine with $\beta = 0.2$ | 2.9 |
| PAM | Root-raised-cosine with $\beta = 0.1$ | 3.7 |
| PAM* | Root-raised-cosine + pre-emphasis filter | 3.1 |
| CAP | Root-raised-cosine with $\beta = 0.2$ | 2.4 |
| OMM | Coded pulses | 0 |

* Assuming 4-PAM and modulator bandwidth of 30 GHz.

The dc bias is particularly important as it determines the average optical power at the modulator output. The minimum required dc bias for the driver signal is equal to minimum negative excursion of the signal at the output of the DAC. Ignoring distortion caused by the anti-aliasing filter and finite DAC resolution, we have

$$\bar{P} = - \min_{\{a_k\},t} \sum_n \sum_{k=1}^{N} a_n^{(k)} g^{(k)} \left( t - nT_s \right). \qquad (14)$$

The minimum occurs when the largest symbols, i.e., $\pm (M-1)$ are sent. Hence,

$$\bar{P} = (M - 1) \cdot \max_t \sum_n \sum_{k=1}^{N} \left| g^{(k)} \left( t - nT_s \right) \right|. \qquad (15)$$

By normalizing (15), we can quantify the pulse shaping penalty as

$$\Delta \bar{P}_{shaping} = \frac{1}{N} \cdot \max_t \sum_n \sum_{k=1}^{N} \left| g^{(k)} \left( t - nT_s \right) \right|, \qquad (16)$$

and we can rewrite (4) as

$$\frac{\overline{P}_{req}}{\overline{P}_{OOK,req}} = (M - 1) \sqrt{\frac{N}{log_2 M}} \cdot \Delta \bar{P}_{shaping}. \qquad (17)$$

Table I summarizes the pulse shaping penalty for different pulse shapes. Note that pre-emphasis filter, while significantly reducing the interference caused by the modulator, increases the required optical power by 3.1 dB, which is much more than the penalty obtained using receiver-side equalization.

Fig. 7 shows the optical power penalty for 4-PAM with different pulse shapes. It can be seen that in systems with pulse shaping, the power penalty arises mainly from pulse shaping penalty, rather than interference. Hence, one should avoid non-rectangular pulse shaping unless it is necessary, such as with CAP modulation.

### IV. SYSTEM COMPLEXITY

In this section, we establish requirements for the resolution and sampling rate of the DAC and ADC. We also evaluate the complexity of the DSP required for various schemes.

Resolution and sampling rate requirements of the DAC/ADC are particularly important, as these components along with the DSP dominate the system power consumption.
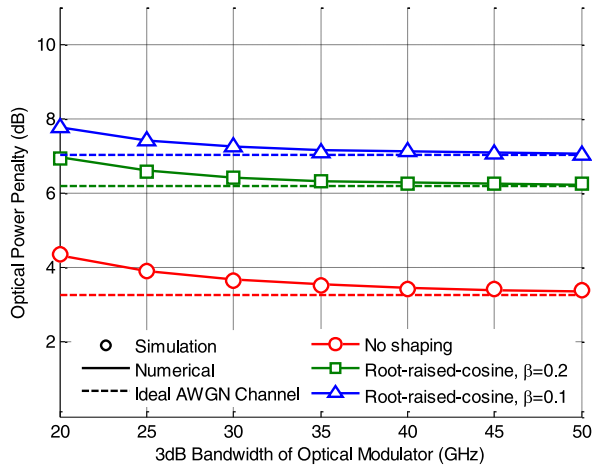
Fig. 7. Normalized optical power penalty for 4-PAM systems with root-raised-cosine pulse shaping using LE.

TABLE II
SAMPLING REQUIREMENTS OF DAC/ADC

| Modulation | M | Symbol rate (GBd) | Sampling rate (GS/s) |
|---|---|---|---|
| M-PAM | 4 | 53.5 | 107 |
|  | 8 | 35.7 | 71.4 |
|  | 16 | 26.8 | 53.6 |
| M- PAM + root-raised cosine* | 4 | 53.5 | 66.9 |
|  | 8 | 35.7 | 44.67 |
|  | 16 | 26.8 | 33.5 |
| 16-CAP* | 4 | 26.8 | 64.3 |
| OMM | 2 | 26.8 | 214 |

*Assuming roll-off factor $\beta = 0.2$.

## A. DAC/ADC

To generate *M*-PAM symbols, a DAC with a minimum resolution of $\log_2 (M)$ bits and sampling at the symbol rate is required. DACs with higher sampling rate and resolution allow for digital pulse shaping and pre-compensation of the modulator frequency response. ADCs are generally characterized by their effective number of bits (ENOB). ADCs with ENOB of 6 and sampling rate as high as 65 GSamples/s are commercially available [4]. Although symbol-rate sampling is sufficient in an ideal optimal receiver, in practice, an oversampling ratio $r_{os}$ slightly above 1 is necessary to compensate for timing errors and inaccurate estimation of the channel. Note that a FSE employing sub-Nyquist sampling rate might still be susceptible to sampling time errors. Hence, it is best to sample the received signal above the Nyquist rate. As an example, for root-raised-cosine shaping with roll-off factor $\beta$, the Nyquit sampling rate is given by

$$f_{ADC} > 2\left(1 + \beta\right)/T_s. \qquad (18)$$

For rectangular pulse shapes, an oversampling ratio $r_{os}$ above 2 is sufficient to make aliasing effects negligible. Table II summarizes the symbol rates and the sampling rates assuming minimum oversampling of $r_{os} = 5/4$ for various schemes. Note that the sampling rate for OMM is prohibitively high, which

makes analog implementation the only viable realization of this scheme.

The resolution required of the DAC and ADC are important, as the precision of the samples affects DSP performance. For systems without digital pulse, shaping such as standard PAM, ADC has more stringent requirements than the DAC. Hence, we focus on the ADC resolution requirements. Finite ADC precision introduces additional additive noise to the samples, which is typically modeled by a uniform distribution [27]. Therefore, we model quantization as an additive white noise uniformly distributed between $\pm b$ with variance of $b^2/3$, where $b$ is half the ADC level spacing. Assuming an ADC with resolution of *ENOB* and dynamic range of $\Delta X_{ADC}$, we can write the noise variance as

$$\sigma_Q^2 = \frac{\Delta X_{ADC}}{12 \cdot 2^{\text{ENOB}}}. \qquad (19)$$

The quantization noise variance is proportional to the dynamic range of the converter. Hence, efficient use of the ADC requires some degree of scaling and clipping of the signal to reduce the dynamic range of ADC. The threshold of clipping is normally quantified by a clipping ratio

$$r = \frac{\Delta X_{ADC}}{2\sigma}, \qquad (20)$$

where $\sigma$ is the standard deviation of the transmitted signal. Clipping, while reducing the quantization noise, introduces signal-dependent clipping noise. The optimal clipping ratio depends on the modulator response and the input signal statistics. We empirically optimize the clipping ratio at each modulator bandwidth to minimize the optical power penalty. As a general guideline, the dynamic range of the ADC should be higher than the dynamic range of the signal in the absence of thermal noise, which is given by

$$\Delta X_{signal} = 2\left(M - 1\right) \sum_{i,j} \sum_{l=0}^{L} \left| x_l^{(ij)} \right|. \qquad (21)$$

Fig. 8 shows the optical power penalty of *M*-PAM for different ENOB values. As expected, higher PAM orders require higher resolution. We observe that 4-PAM can be implemented with an ADC ENOB as low as 5 bits with almost no power penalty, which is advantageous for low-power data center links. ADCs with ENOB of 5 bits are more desirable as they can be implemented using s flash architecture, which has low power consumption, and has no error floors [4].

It is worth mentioning that quantization is only important in systems using DSP. In the absence of bandwidth limitations and digital equalization, one can minimize quantization noise by aligning the ADC levels with PAM levels.

## B. DSP Complexity

One of the major challenges of 100G links is performing DSP at a high speed, so it is worth studying the complexity of digital equalization. We quantify equalization complexity by the number of complex multiplications per transmitted data symbol, assuming the channel is known a priori.
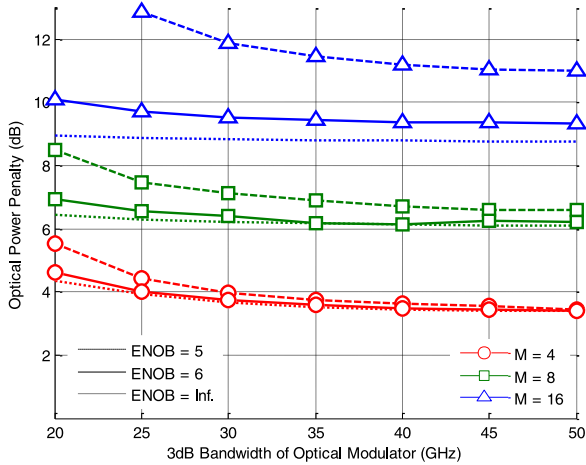
Fig. 8.    Normalized optical power penalty for PAM systems with different ADC resolutions using LE.
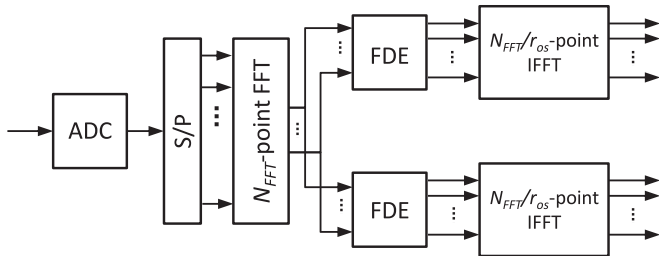


Fig. 9.    Block diagram of fixed frequency-domain equalization of an OPAM system with two subchannels.
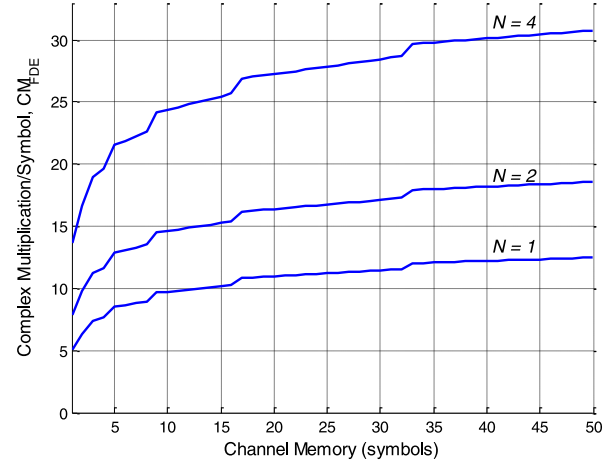


Fig. 10.    Number of complex multiplication as a function of channel memory length measured in symbol intervals for frequency-domain LE of 4-PAM.

We consider performing the FFT and inverse FFT (IFFT) efficiently using a radix-2 algorithm, which requires approximately $N_{FFT} \lceil \log_2 (N_{FFT}) \rceil /2$ complex multiplications.

Note that, in practice, arbitrary $r_{os}$ may not be achievable using power-of-two FFT sizes. Using the aforementioned approximation, we estimate the required number of complex multiplications per symbol to be

$$CM = \frac{1}{N_{FFT} - N_{overlap}} \{ N N_{FFT}$$
$$+ \frac{1}{2} r_{os} N_{FFT} \log_2 (N_{FFT})$$
$$+ \frac{N}{2} N_{FFT} \log_2 \lceil N_{FFT}/r_{os} \rceil \} \qquad (22)$$

where the first term corresponds to channel inversion and the second and third terms are for FFT/IFFT operations.

Fig. 10 shows the complexity of linear FDE as a function of the channel memory length measured in symbol intervals. The FFT block length is assumed to be the smallest power of two greater that eight times the channel length [29]. For FFT sizes of 64-256, the latency of FDE is 1–10 ns depending on the baud rate, while the latency of FEC decoders for 100G links is more than 100 ns [21]. Hence, FDE has a negligible impact on receiver latency, which is dominated by FEC decoding.

In the absence of accurate channel estimation, the FDE coefficients must be computed iteratively. For an adaptive FDE, the least mean squares algorithm can be used to minimize the frequency error [30]. During adaptation, $2N_{FFT}$ extra multiplications are required for calculating the frequency error and updating the coefficients.

As was shown in the previous section, LE has a comparable performance to DFE and MLSD with lower complexity. Hence, we focus on systems using a feedforward LE. We consider linear frequency-domain equalization (FDE), as it has lower computational complexity than its time-domain. Counterpart [28], [29]. In FDE, equalization is done by performing a fast Fourier transform (FFT) on a block of $N_{FFT}$ samples and inverting the channel in the frequency domain. One approach to process each block independently is prepending a cyclic prefix of length $N_{CP}$ to each block of $N_{FFT}/r_{os}$ symbols before transmission. The cyclic prefix is then discarded at the receiver before the FFT operation. The cyclic prefix also simplifies realization of an adaptive FDE [30]. However, using a cyclic prefix reduces the throughput and the average power efficiency.

A second approach, adopted here, is to use overlap-save or overlap-add convolution to avoid the cyclic prefix overhead [31], [32]. In the overlap-save method, used here, the FFT is performed on sliding windows of $N_{FFT}$ samples. After equalization, overlapped samples are discarded from the equalized samples, and the remaining equalized samples are down-sampled to the symbol rate. To reduce the complexity of FDE, unlike previous works [13], down-sampling is realized by discarding high-frequency components of the signal. Therefore, IFFT size can be a factor of $r_{os}$ smaller than the FFT size.

## C. Coding

Due to the tight power budge of the 100G links, we have considered coded systems with coding gain of about 5dB. For interconnects application, complexity, latency, and over-clocking requirements are as important as the coding gain in selection of the FEC. References [21] and [33] highlight FEC requirements for 100G applications.

## V. OVERALL SYSTEM PERFORMANCE

In this section, we evaluate the performance of WDM-based 400G links in the presence of linear and nonlinear fiber and modulator impairments. We assume four WDM channels operating near the zero-dispersion wavelength (1310 nm). We assume coarse wavelength-division multiplexing (CWDM) with 20-nm channel spacing to avoid the need for laser temperature stabilization [34]. We further assume an optical modulator with 3-dB bandwidth of 30 GHz. The performance obtained using this modulator depends on the characteristics of laser frequency chirp. The phase shift for transient chirp-dominated DMLs or EAMs can be expressed as

$$\Delta\phi\left(t\right) \approx \frac{\alpha}{2}\ln\left(p\left(t\right)\right), \qquad (23)$$

where $\alpha$ is the chirp parameter. For commercially available modulators, $\alpha$ is about 2–4 [35], [36]. Using (23) the dispersion-induced frequency response of the channel excluding the fiber loss is described by

$$H\left(f, L_{fiber}\right) \approx \sqrt{1+\alpha^2}cos\left(\theta_d\left(2\pi f\right)^2 - \theta_\alpha\right), \qquad (24)$$

where $L_{fiber}$ is the fiber length, $\theta_\alpha = \tan^{-1}\alpha$, and $\theta_d = 1/2\beta_2 L_{fiber}$. Based on (24), systems with $\alpha\beta_2 < 0$ are subject to power fading. Hence, we assume the WDM channels are operating at wavelengths shorter than the zero-dispersion wavelength, such that $\alpha\beta_2 > 0$. We focus on the performance of the sub-channel at 1250 nm, as it is subject to the highest dispersion and hence has the worst performance.

Nonlinearity of the modulator is modeled by inserting an instantaneous nonlinear voltage-to-intensity transfer characteristic governed by

$$P_{out}(t) = P_{in}10^{-\alpha_{dB}\left(V(t)\right)/10}, \qquad (25)$$

after the linear filter representing the modulator frequency response. The EAM dynamic absorption $\alpha_{dB}(V)$ is modeled using a cubic spline fit to experimental data from Fig. 4 in [37]. To compensate for the nonlinearity, the level spacing at the DAC is adjusted based on the inverse of the modulator transfer characteristic, but no attempt is made to compensate at the transmitter for the modulator's linear frequency response.

We only consider 4-PAM, as it has the lowest power penalty and complexity among techniques considered. Assuming a bit rate of 107 Gb/s (including 7% coding overhead), the symbol rate of a 4-PAM system is 53.5 GBd. Table III summarizes other parameters used in the simulation.

Fig 11 shows the optical power penalty versus the optical fiber length. The 5-dB gap between the penalty obtained using the discrete-time model and based on simulation of a back-to-back system is mostly caused by the non-ideal extinction ratio, nonlinearity of the modulator, finite resolution and frequency response of the ADC and DAC, and sub-Nyquist sampling rate of ADC. Intensity noise, and shot noise, while important for higher order modulation [6], [14], have a negligible impact on the performance of 4-PAM.

We further observe that for short fibers up to 2 km, modulator chirp and CD have a small impact on system performance. As

TABLE III
SIMULATION PARAMETERS

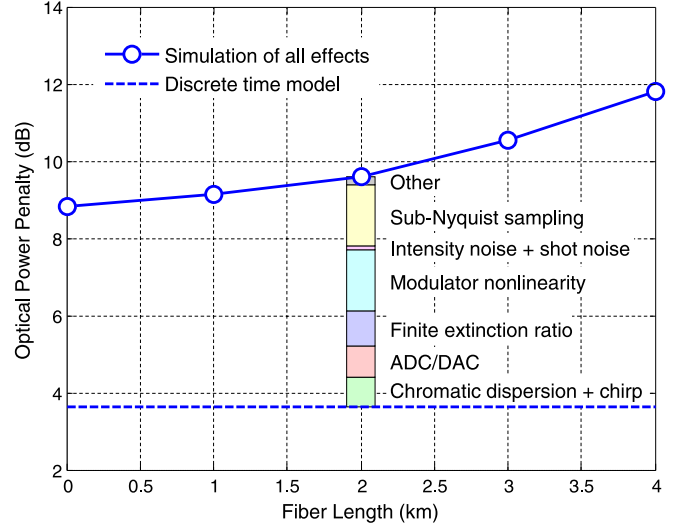| | | |
|---|---|---|
| DML | $f_{3dB}$ | 30 GHz |
| | $\lambda$ | 1250 nm |
| | RIN | $-150$ dB/Hz |
| | $\alpha$ | 2 |
| SMF | $S_0$ | 0.092 ps/(nm$^2 \cdot$ km) |
| TIA | $I_{n,in}$ | 30 pA/$\sqrt{\text{Hz}}$ |
| ADC | $r_{os}$ | 1.28 |
| | ENOB | 5 |
| FDE | $N_{FFT}$ | 128 |
| | $N_{overlap}$ | 16 |



Fig. 11. Optical power penalty versus fiber length for a 4-PAM system using LE. Solid line: simulation including all impairments. Dashed line: based on discrete-time model for thermal noise-dominated receiver, as described in Section III. Colored bars: penalties from individual impairments at fiber length of 2 km.

we increase the fiber length, the combined effects of chirp and CD cause severe nonlinear distortion, which cannot be compensated by LE. Fortunately, data center applications target fiber lengths up to about 2 km, where nonlinear distortion from CD is negligible.

## VI. CONCLUSION

We have evaluated the performance and complexity of single-carrier modulation schemes for data center interconnects. We evaluated performance using analysis and simulation based on a discrete-time model. We highlighted the system design trade-offs including equalization complexity, modulation order, and number of subchannels. We further established requirements for DAC/ADC resolution and sampling rates.

Among single carrier schemes, we found 4-PAM to be the most promising scheme for short-reach data center interconnects, as it has the lowest optical power penalty. It can be realized using ADCs with ENOB as low as 5 bits. We have presented the simulation results for a 4-PAM system in the presence of CD, nonlinearity and non-ideal extinction ratio of the modulator, finite resolution and frequency response of the ADC

and DAC, intensity noise, shot noise, and quantization noise. Most of these impairments have an impact that increases as the modulation order is increased, which further favors 4-PAM for data center interconnects. We have shown nonlinear distortion caused by dispersion and chirp has a negligible impact for fiber lengths up to 2 km. However, for longer distances, nonlinear distortion becomes problematic, as it cannot be compensated by LE.

We have verified that 4-PAM can meet the optical power requirement imposed by eye safety. Assuming a 4-channel CWDM system with 5-dB link attenuation, 4-PAM has a power margin of about 4.9 dB for 2-km links. As we have shown here and in the companion, paper both single and multiple carrier systems have a small power margin, and further research is required to improve the power margin for short reach data center interconnects.

### Appendix A
### Power Spectral Density of Orthogonal Multi-Pulse Modulation

In can be shown [23] that $s(t)$ is a cyclostationary random process with a power spectral density

$$S_s(f) = \frac{E[a_n^2]}{T_s} \sum_{i=1}^{N} |G_i(f)|^2. \qquad (26)$$

For OMM, the $i$th pulse shape can be expressed as

$$g_i(t) = \sum_{l=1}^{N} c_{il} \Pi\left(\frac{N}{T_s}t - (l-1)\right), \qquad (27)$$

where $\Pi(t)$ is a rectangular pulse of unit duration and $C$ is a code matrix, whose columns are mutually orthogonal. By taking the Fourier transform of (25) we obtain

$$G_i(f) = \sum_{l=1}^{N} c_{il} \frac{T_s}{N} \mathrm{sinc}\left(\frac{T_s f}{N}\right) e^{\frac{j2\pi f T_s (l-1)}{N}}. \qquad (28)$$

Hence

$$|G_i(f)|^2 = \left(\frac{T_s}{N}\right)^2 \mathrm{sinc}^2\left(\frac{T_s f}{N}\right)$$
$$\sum_{k,l=1}^{N} c_{ik} c_{il} \cos\left(\frac{2\pi f T_s (l-k)}{N}\right). \qquad (29)$$

By substituting (27) in (24) we have

$$S_s(f) = \frac{E(a_n^2) T_s}{N^2} \mathrm{sinc}^2\left(\frac{T_s f}{N}\right)$$
$$\sum_{i,k,l=1}^{N} c_{ik} c_{il} \cos\left(\frac{2\pi f T_s (l-k)}{N}\right). \qquad (30)$$

The columns of $C$ are mutually orthogonal. Hence

$$\sum_{i}^{N} c_{ik} c_{il} = \begin{cases} N & \text{if } k = l \\ 0 & \text{o.w.} \end{cases} \qquad (31)$$

Using (29) the power spectral density can be simplified to

$$S_s(f) = T_s \mathrm{sinc}^2\left(\frac{T_s f}{N}\right), \qquad (32)$$

which is the same as the power spectral density of OOK with the same bit rate.

### References

[1] C. Cole, "Beyond 100G client optics," *IEEE Commun. Mag.*, vol. 50, no. 2, pp. 58–66, Feb. 2012.
[2] R. Gutierrez-Castrejon and P. Torres-Ferrera, "Design and technical feasibility of next 400 GbE 40-km PMD based on 16×25 Gbps architecture," *J. Lightw. Technol.*, vol. 31, no. 14, pp. 2386–2393, Jul. 2013.
[3] P. J. Winzer, "High-spectral-efficiency optical modulation formats," *J. Lightw. Technol.*, vol. 30, no. 24, pp. 3824–3835, Dec. 2012.
[4] C. Cole, I. Lyubomirsky, A. Ghiasi, and V. Telang, "Higher-order modulation for client optics," *IEEE Commun. Mag.*, vol. 51, no. 3, pp. 50–57, Mar. 2013.
[5] A. Ghiasi, Zh. Wang, and V. Telang, "Investigation of PAM-4/6/8 signaling and FEC for 100 Gb/s serial transmission," IEEE 802.3bm Task Force, Geneva, Switzerland, Sep. 2012.
[6] G. Nichol and C. Fludger, "Update on technical feasibility for PAM modulation," IEEE 802.3 NG100GE PMD Study Group, Mar. 2012.
[7] J. L. Wei, D. G. Cunningham, R. V. Penty, and I. H. White, "Study of 100 Gigabit ethernet using carrierless amplitude/phase modulation and optical OFDM," *J. Lightw. Technol.*, vol. 31, no. 9, pp. 1367–1373, May 2013.
[8] M. I. Olmedo *et al.*, "Multiband carrierless amplitude phase modulation for high capacity optical data links," *J. Lightw. Technol.*, vol. 32, no. 4, pp. 798–804, Feb. 2014.
[9] W. A. Ling, I. Lyubomirsky, and O. Solgaard, "Digital quadrature amplitude modulation with optimized non-rectangular constellations for 100 Gb/s transmission by a directly-modulated laser," *Opt. Exp.*, vol. 22, no. 9, pp. 10844–10857, 2014.
[10] J. D. Ingham, R. V. Penty, and I. H. White, "Orthogonal multipulse modulation in optical data communications," presented at the Int. Conf. Transport Optical Networks, Cartagena, Spain, 2013.
[11] J. L. Wei, Q. Cheng, R. V. Penty, I. H. White, and D. G. Cunningham, "400 gigabit ethernet using advanced modulation formats: Performance, complexity, and power dissipation," *IEEE Commun. Mag.*, vol. 53, no. 2, pp. 182–189, Feb. 2015.
[12] J. L. Wei, J. D. Ingham, D. G. Cunningham, R. V. Penty, and I. H. White, "Comparison of 100 Gb/s Ethernet links using PAM-8, multipulse, and hybrid CAP-16/QAM-16 modulation schemes," presented at the 39th European Conf. Optical Commun., London, U.K., 2013.
[13] K. Zhong *et al.*, "Experimental study of PAM-4, CAP-16, and DMT for 100 Gb/s short reach optical transmission systems," *Opt. Exp.*, vol. 23, no. 2, pp. 1176–1189, 2015.
[14] J. K. Perin, M. Sharif, and J. M. Kahn, "Modulation schemes for single-wavelength 100 Gbits/s links: multicarrier," *J. Lightw. Technol.*, submitted for publication
[15] S. Bhoja, "Study of PAM modulation for 100GE over a single laser," IEEE Next Gen 100G Optical Ethernet Study Group, Newport Beach, Jan. 2012.
[16] J. L. Wei, L. Geng, D. G. Cunningha, R. V. Penty, and I. H. White, "100 gigabit ethernet transmission enabled by carrierless amplitude and phase modulation using QAM receivers," presented at the Optical Fiber Commun./Nat. Fiber Opt. Electron. Conf., Anaheim, CA, USA, 2013.
[17] J. Kreissl *et al.*, "Up to 40 Gb/s directly modulated laser operating at low driving current: Buried-heterostructure passive feedback laser (BH-PFL)," *IEEE Photon. Technol. Lett.*, vol. 24, no. 5, pp. 362–364, Mar. 2012.
[18] N. Kikuchi, R. Hirai, and T. Fukui, "Practical implementation of 100-Gbit/s/lambda optical short-reach transceiver with Nyquist PAM4 signaling using electroabsorptive modulated laser (EML)," presented at the Optical Fiber Communication Conf., Los Angeles, CA, USA, 2015.
[19] G. Ghione, *Semiconductor Devices High-Speed Optoelectronics.* Cambridge, U.K.,: Cambridge Univ. Press, 2009.

[20] J. R. Barry, *Wireless Infrared Communication*. New York, NY, USA: Springer, 1994.

[21] S. Bates *et al.*, "FEC options," IEEE P802.3bj, Newport Beach, 2011.

[22] *Safety of Laser Products—Part 1: Equipment Classification and Requirements*, Standard IEC60825-1, 2014.

[23] J. Proakis and M. Salehi, *Digital Communication*. New York, NY, USA: McGraw-Hill, 2007.

[24] G. D. Forney, "Maximum-likelihood sequence estimation of digital sequences in the presence of intersymbol interference," *IEEE Trans Inf. Theory,*, vol. 18, no. 3, pp. 363–378, May 1972.

[25] A. Duel-Hallen, J. Holtzman, and Z. Zvonar, "Multiuser detection for CDMA systems," *IEEE Personel Commun.*, vol. 2, no. 2, pp. 46–58, Apr. 1995.

[26] J. G. Andrews, "Interference cancellation for cellular systems: A contemporary overview," *IEEE Wireless Commun.*, vol. 12, no. 2, pp. 19–29, Apr. 2005.

[27] B. Widrow, I. Kollar, and Ming-Chang Liu, "Statistical theory of quantization," *IEEE Trans. Instrum. Meas.*, vol. 45, no. 2, pp. 353–361, Apr. 1996.

[28] D. Falconer, S. L. Ariyavisitakul, A. Benyamin-Seeyar, and B. Eidson, "Frequency domain equalization for single-carrier broadband wireless systems," *IEEE Commun. Mag.*, vol. 40, no. 4, pp. 58–66, Apr. 2002.

[29] D. D. Falconer and S. L. Ariyavisitakul, "Broadband wireless using single carrier and frequency domain equalization," in *Proc. 5th Int. Symp. Wireless Personel Multimedia Commun.*, vol. 1, Honolulu, HI, USA, 2002, pp. 27–36.

[30] M. V. Clark, "Adaptive frequency-domain equalization and diversity combining for broadband wireless communications," presented at the Vehicular Technology Conf., Ottawa, ON, Canada, 1998.

[31] T. Kobayashi *et al.*, "Frequency-domain equalisation without guard interval for optical transmission systems," *Electron. Lett.*, vol. 44, no. 25, pp. 1480–1482, 2008.

[32] S. Haykin, *Adaptive Filter Theory*. Upper Saddle River, NJ, USA: Prentice-Hall, 2002.

[33] Z. Wang and A. Ghiasi, "FEC tradeoffs and analysis for 100G optical networking," Geneva, Switzerland, 2012.

[34] C. F. Lam, H. Liu, and R. Urata, "What devices do data centers need?," presented at the Opt. Fiber Communication Conf., San Francisco, CA, USA, 2014, Paper M2K.5.

[35] Y. Cheng *et al.*, "40-Gb/s low chirp electroabsorption modulator integrated with DFB Laser," *IEEE Photon. Technol. Lett.*, vol. 21, no. 6, pp. 356–358, Mar. 2009.

[36] A. Villafranca, J. A. Lazaro, I. Salinas, and I. Garces, "Measurement of the linewidth enhancement factor in DFB lasers using a high-resolution optical spectrum analyzer," *IEEE Photon. Technol. Lett.*, vol. 17, no. 11, pp. 2268–2270, Nov. 2005.

[37] A. D. Gallant and J. C. Cartledge, "Characterization of the dynamic absorption of electroabsorption modulators with application to OTDM demultiplexing," *J. Lightw. Technol.*, vol. 26, no. 13, pp. 1835–1839, Jul. 2008.

[38] A. Maruf Newaz, "Transimpedance amplifier (TIA) design for 400 Gb/s optical fiber communications," PhD Dissertation, Virginia Polytechnic Institute and State University, 2013.

Authors' biographies not available at the time of publication